Microfabricated Optically-Pumped Magnetometers for Biomagnetic Applications

Svenja Knappe, Orang Alem, Dong Sheng, John Kitching

NIST, 325 Broadway, Boulder CO 80305, USA

Email: knappe@nist.gov

Abstract. We report on the progress in developing microfabricated optically-pumped magnetometer arrays for imaging applications. We have improved our sensitivities by several orders of magnitude in the last ten years. Now, our zero-field magnetometers reach noise values below 15 fT/Hz$^{1/2}$. Recently, we have also developed gradiometers to reject ambient magnetic field noise. We have built several imaging arrays and validated them for biomedical measurements of brain and heart activity.

1. Introduction

Sensors based on laser spectroscopy of atoms have shown impressive precision in the laboratories [1, 2]; atom-based gyroscopes have reached angle-random walks (ARW) of 2×10^{-6} °/√h [3], cold-atom gravimeters have shown sensitivities of $\Delta g/g = 8 \times 10^{-9}$ [4], and atomic magnetometers have reached 160 aT/Hz$^{1/2}$ sensitivity [5]. These levels of performance have opened new opportunities for atom-based sensors in real-world applications and as a result, several companies are now trying to commercialize these advanced sensor approaches. In a commercial setting, especially when high-volume manufacturing is desirable, the challenges of robustness, reliability, and cost must be addressed. The use of microfabrication techniques commonly used in microelectronics and microelectromechanical systems (MEMS) can offer significant advantages for manufacturing and in addition enable improvements in device size, weight and power. Microfabrication has been successfully implemented in commercially available atomic vapor cell clocks [6].

2. Overview of microfabricated optically-pumped magnetometers

Optically-pumped magnetometers have been developed since the 1960s [7, 8], where near-resonant light creates atomic polarization in the ground state of the atoms. The resultant Larmor spin precession can be detected with near-resonant light and serves as a measure of the ambient magnetic field.

Our group developed the first chip-scale optically-pumped magnetometer in 2004 [9]. A thermal vapor of ^{87}Rb atoms was confined in a MEMS vapor cell [10] with an internal volume of 1 mm^3. It utilized coherent population trapping (CPT) to interrogate the atoms on a magnetically-sensitive hyperfine transition. A vertical-cavity surface-emitting laser (VCSEL) was integrated with micro-optics on the sensor head directly, which had a volume of 10 mm^3 without packaging (Figure 1, 2004, green online). The magnetometer reached a sensitivity, i.e., a noise equivalent magnetic field, of 50 pT/Hz$^{1/2}$ at 10 Hz.

By changing to spectroscopy of a Zeeman transition, the spin-destruction collision rate could be reduced and the resonance contrast enhanced, which resulted in a factor of ten improvement in sensitivity [11] (Figure 1, 2006, blue online). The physics package of this device was very similar to

the previous one, but it included a pair of field coils to drive the Zeeman resonance magnetically instead of optically. In this so-called Mx configuration, the transmission signal is detected phase-sensitively at the Larmor frequency. Alternatively, we have operated similar magnetometers in an all-optical mode as well as the Mz mode, with similar sensitivities of 5 pT/Hz$^{1/2}$. For microfabricated scalar magnetometers, sensitivity could be increased by implementing a balanced polarimeter [12, 13], a multipass cell [14], or through light narrowing [15].

Higher sensitivities can be achieved when decoherence due to spin-exchange collisions can be suppressed [16] by operating in a regime where the spin-exchange collision rate is faster than the Larmor precession frequency [17]. This limits the dynamic range of the magnetometer, but it could still be useful for biomedical applications, where high sensitivities are required in magnetically-shielded environments. In a tabletop setup, we measured sensitivities around 70 fT/Hz$^{1/2}$ in a MEMS vapor cell of 2 x 3 x 1 mm^3 volume [18] (Figure 1, 2007, grey online). The configuration was simplified by using a single circularly-polarized beam [8] to replace two perpendicular beams of a standard pump-probe configuration [16]. In order to be sensitive to a component of the magnetic field perpendicular to the laser beam, a small oscillating magnetic field is applied in that direction and the transmission signal is detected phase-sensitively. The sensitivity of the magnetometer in this configuration will fundamentally be limited by photon shot noise, which can be replaced by atomic spin projection noise when using separate pump and probe laser beams.

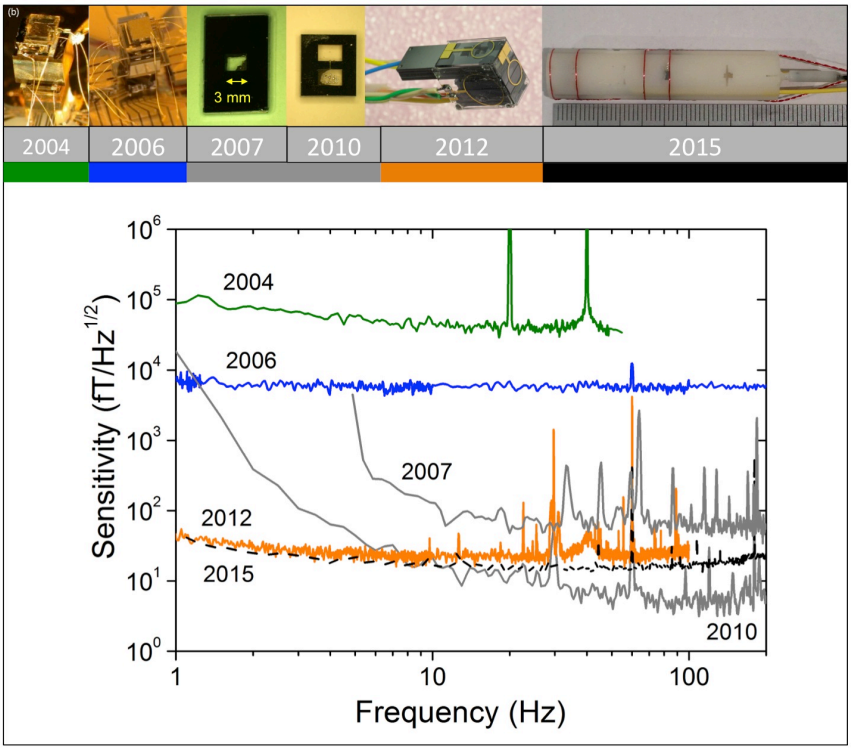

Figure 1: (Bottom) Sensitivity for several generations of our magnetometers. The grey lines are tabletop measurements. (Top) Photographs of the same MEMS magnetometers (colour online).

In a more complicated tabletop setup, a circularly-polarized near-resonant pump laser was split into two arms to optically pump ^{87}Rb atoms in a MEMS vapor cell to create a uniform spin-polarization. A further detuned linearly-polarized probe laser was incident on the cell perpendicular to the pump beam. The polarization rotation of the probe beam was measured with a balanced polarimeter. In a 1 mm^3 volume, we have measured sensitivities as low as 5 fT/Hz$^{1/2}$ (Figure 1, 2010, grey online).

So far, we have built fully packaged sensor heads in single-beam geometries only. For biomedical imaging applications, where large arrays of sensors are needed, we have chosen a design of fiber-coupled sensors heads: A distributed-feedback laser (DFB) is split into up to 16 channels and coupled to the individual sensor heads. We have reached sensitivities between 15 to 20 fT/Hz$^{1/2}$, when averaged between 10 Hz and 50 Hz, in cells with inner volumes of (1.5 mm)^3 (Figure 1, 2012, orange online).

3. Fabrication of microfabricated optically-pumped magnetometers

For biomagnetic imaging applications, the sensor heads are coupled to a control unit through 5 m long optical fibers. That way, the control system can remain outside the shielded room and the sensor heads with footprints of roughly 1 cm^2 are fed to the inside of the room through small holes in the shield. At the heart of the sensor heads are microfabricated alkali vapor cells [10]. Dimensions vary between 1 mm and 4 mm, depending on the application requirements (Figure 2a). These cells have to be heated to roughly 150 °C, while the outside of the package has to remain at room temperature, since it might be directly placed on the skin of a subject.

For this purpose, we have developed low-power MEMS vacuum packages [19] based on anodic bonding of silicon and glass (Figure 2b). The cells are heated optically; glass filters are placed onto the windows of the cell, and light from a second laser at 1550 nm is absorbed by these filters. To reduce conductive heat losses below 5 mW, the cell of volume (1.5 mm)^3 is placed onto a web of polyimide attached to a silicon frame [20]. The radiative heat losses are dominating with roughly 50 mW. When additional gasses are present inside the vacuum package, the required heating power increases due to a convective contribution, which was the case in many of our earlier packages.

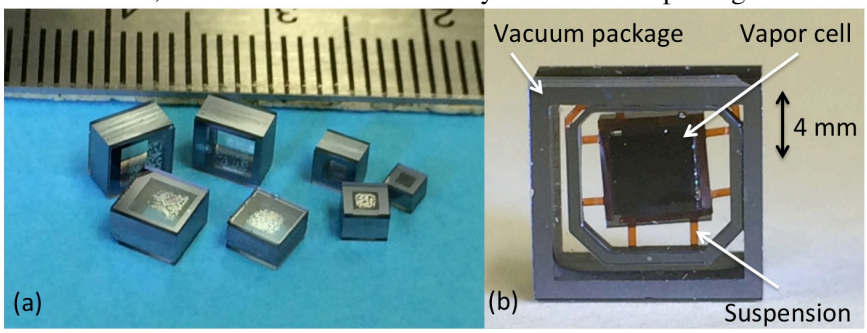

Figure 2: (a) Photograph of several MEMS alkali vapor cells. (b) Photograph of a low-power MEMS vacuum package.

4. Noise contributions

The fundamental performance limits of the single-beam zero-field magnetometers are given by the spin-projection noise and photon shot noise. Under our operating conditions, these noise contributions are usually under 1 fT/Hz$^{1/2}$ and 10 fT/Hz$^{1/2}$, respectively. Besides these fundamental contributions, additional noise sources fall into the categories of laser noise, magnetic noise, and technical noise. As technical noise, we consider contributions from electronics, currents on the magnetic field coils, and vibrations of the sensors in a magnetic gradient environment.

Fluctuations in the intensities, frequencies, and polarizations of the pump and heat lasers can affect the position and shape of the resonance line. By locking the sensor to the peak of the magnetic resonance, rather than running the magnetometer open loop, contributions of the lasers, which do not cause frequency shifts, can be eliminated. This is done by feeding an error signal, generated from the magnetic resonance signal, back to compensating field coils, which are printed onto flexible circuits wrapped around the sensor heads. Field coils must be designed carefully to minimize cross-talk between different sensors in a dense array and this problem still requires more future work.

The largest laser noise contribution of roughly10 fT/Hz$^{1/2}$ stems from laser intensity fluctuations. A major laser contribution that generates fluctuations of the resonance position is the AC Stark shift

from the pump laser. The laser is circularly polarized, which will shift the Zeeman levels similar to a magnetic field [21, 22]. Since the laser is locked to the center of the optical resonance, there is no large DC magnetic field offset, but laser frequency fluctuations can be interpreted as magnetic field fluctuations in the direction of the laser beam. In many of our compact designs, the laser is not collimated, which can cause fluctuations in the sensitive direction of the magnetometer. In these cases the laser frequency has to be carefully stabilized in order not to increase the noise equivalent magnetic field at low frequencies.

Finally, magnetic field noise from components with high electrical conductivity or permeability in the proximity of the atoms has to be considered [23]. Calculations of the noise from our mu-metal enclosure suggest noise levels of 10 fT/Hz$^{1/2}$ at 1 Hz and 3 fT/Hz$^{1/2}$ at 100 Hz. Therefore, we added an inner magnetic shield made of a ferrite with an estimated noise of 2 fT/Hz$^{1/2}$ at 1 Hz [24]. We estimate noise from silicon cell walls to be 3 fT/Hz$^{1/2}$, if the standard low-resistivity silicon is used. This can be reduced to 0.01 fT/Hz$^{1/2}$ by use of silicon with a resistivity of 8 kΩ·cm [25]. Our calculations suggest that excess Rb metal on the cell walls could also have significant contribution to magnetic noise; a Rb sphere of diameter 100 μm at a distance of 0.5 mm would create magnetic noise of 7 fT/Hz$^{1/2}$, and a 1 nm thick Rb film on the walls of a 1 mm^3 cell would cause 3 fT/Hz$^{1/2}$ noise in the center of the cell [25]. We have therefore fabricated cells with internal reservoirs to keep the solid Rb metal further away from the interrogation region. While we have identified and mitigated many contributions to our magnetometer noise, the noise budget at frequencies below 10 Hz is still under investigation.

5. Gradiometers

One standard technique to suppress ambient magnetic noise is to operate magnetic field sensors in a gradiometer mode. This is done by placing two magnetometers a certain distance, called the baseline, from each other. When subtracting the outputs of the two magnetometers, readings from far away sources and homogeneous fields will be suppressed by a factor called the common mode rejection ratio (CMRR). In many real-world applications there are large amounts of magnetic background noise and the development of efficient gradiometers is of importance. We have built a gradiometer with two cells separated by 2 cm on the same sensor head. In order to minimize noise contributions from the pump laser, one laser beam is split into two arms on the sensor head and detected with two photodiodes. That way, the photon-shot-noise contributions are increased, but the laser amplitude noise contribution is reduced. Since both of these effects contribute equally to our noise, the noise of one magnetometer is similar to the noise measured when two magnetometer signals are subtracted: 15 fT/Hz$^{1/2}$ between 10 and 50 Hz.

In order to reach a high CMRR, both magnetometers are separately operated under negative feedback, where they are locked to the center of the magnetic resonance. This method eliminates scale factor drifts as a result of changing laser parameters. It also eliminates current noise from a global compensation coil system, which can be used to bring the ambient field into the nanotesla range. The major limitation is currently posed by aligning the sensitive axes of the two magnetometers precisely.

6. Biomagnetic Measurements

Highly sensitive magnetometers are used in a variety of biomedical applications. Often, the magnetic fields on the outside of the body are recorded, which are the result of small currents inside the body. In order to localize the sources, a non-unique inverse problem has to be solved. Currently, low-temperature superconducting quantum interference device (SQUID) magnetometers are the only sensors that are used clinically for these applications, since commercial SQUIDs can reach sensitivities around 3 fT/Hz$^{1/2}$. As a result, these imaging systems have a large Dewar as their defining feature, which houses the magnetometer array. It imposes a rigid sensor geometry, makes these systems expensive, and requires high maintenance. It also limits the system's spatial resolution, since the thermal isolation places the SQUID sensors several centimeters from the Dewar surface.

We have developed several multi-channel imaging systems with microfabricated optically-pumped magnetometer sensor heads and have cross-validated them against SQUIDs for biomagnetic

measurements. We have recorded magnetocardiograms (MCG) by placing several sensors over the chest of a healthy subject [26]. In this way magnetic field maps can be generated, with patterns that vary during different sections of a beat [27]. We have also recorded fetal MCG with an array of 25 magnetometers and extracted the maternal and fetal heart signals [28]. In both of these measurements, signal amplitudes of the optically-pumped magnetometers were larger than those measured with SQUIDs, mostly due to the closer proximity to the source.

One biomagnetic imaging application that could benefit from small conformal sensor arrays is magnetoencephalography (MEG), which measures the magnetic fields from neural currents by placing sensors on the scalp of the subject. Due to the curvature of the head, rigid helmets do not allow for close proximity of sensors for every head size. Simulation studies by different groups suggest that the localization error could be reduced substantially with a conformal sensor array where distances between sensitive volume and scalp are less than 5 mm, which is the case for our sensors. We have taken several MEG recordings of spontaneous and evoked brain activity with arrays of several sensors [29]. Recently, we have evaluated a 25-channel array by measuring images of a simple coil, a standard head phantom, and healthy human subjects. The sensors were arranged on a flexible helmet such that each sensor could lightly touch a plastic sphere that housed the phantom dipole or the scalp of the subject. One of the difficulties introduced by a flexible conformal array was to exactly determine the positions of every sensor in the array. Future work includes better determination of sensor locations through a series of externally-applied magnetic fields.

There are several other applications in the biomedical field that could also potentially benefit from uncooled flexible sensor arrays. We have made initial demonstrations of magnetic nanoparticle relaxation [26] and remote detection of nuclear magnetic resonance (NMR) [30] with microfabricated optically-pumped magnetometers.

7. Conclusion

We have developed arrays of microfabricated optically-pumped magnetometers. We have cross-validated our MEG and MCG measurements with those from low-temperature SQUID magnetometers. We have built small gradiometer sensor heads with high common-mode rejection ratios to suppress noise from ambient sources. The complete evaluation of our sensor noise is still ongoing and includes fundamental, technical, laser, and magnetic noise.

We thank Susan Schima for help with the MEMS fabrication, John LeBlanc (Draper Labs.) for building sensor heads for the 25-channel system, and Tilmann Sander and Lutz Trahms (PTB) for the biomagnetic measurements. This is a contribution of NIST, an agency of the U.S. government; and is not subject to copyright.

References

[1] Kitching J, Knappe S, Donley EA 2011 *Sensors Journal, IEEE* **11** 1749-58
[2] Kitching J, Knappe S, Gerginov V, Shah V, Schwindt PDD, Lindseth B, et al. 2008 *Proceedings of the Frequency Standards and Metrology Conference* 445-53
[3] Gustavson TL, Landragin A, Kasevich MA 2000 *Classical and Quantum Gravity* **17** 2385-98
[4] Müller H, Chiow SW, Herrmann S, Chu S, Chung KY 2008 *Physical Review Letters* **100** 031101
[5] Dang HB, Maloof AC, Romalis MV 2010 *Appl Phys Lett* **97** 151110
[6] Knappe S, Shah V, Schwindt PDD, Hollberg L, Kitching J, Liew LA, et al. 2004 *Appl Phys Lett* **85** 1460-2
[7] Bloom A 1962 *Appl Opt* **1** 61-8
[8] Dupont-Roc J, Haroche S, Cohen-Tannoudji C 1969 *Phys Lett A* **28** 628-39
[9] Schwindt PDD, Knappe S, Shah V, Hollberg L, Kitching J, Liew L-A, et al. 2004 *Appl Phys Lett* **85** 6409-11

[10] Liew LA, Knappe S, Moreland J, Robinson H, Hollberg L, Kitching J 2004 *Appl Phys Lett* **84** 2694-6
[11] Schwindt PDD, Lindseth B, Knappe S, Shah V, Kitching J 2007 *Appl Phys Lett* **90** 081102
[12] Shah V, Romalis MV 2009 *Phys Rev A* **80** 013416
[13] Johnson C, Schwindt PDD, Weisend M 2010 *Appl Phys Lett* **97** 243703
[14] Sheng D, Li S, Dural N, Romalis MV 2013 *Phys Rev Lett* **110** 160802
[15] Scholtes T, Schultze V, Ijsselsteijn R, Woetzel S, Meyer HG 2011 *Phys Rev A* **84** 043416
[16] Allred JC, Lyman RN, Kornack TW, Romalis MV 2002 *Phys Rev Lett* **89** 130801
[17] Happer W, Tang H 1973 *Phys Rev Lett* **31** 273
[18] Shah V, Knappe S, Schwindt PDD, Kitching J 2007 *Nature Photonics* **1** 649-52
[19] Mhaskar R, Knappe S, Kitching J 2012 *Appl Phys Lett* **101** 241105
[20] Mescher MJ, Lutwak R, Varghese M 2005 *Solid-State Sensors, Actuators and Microsystems, 2005 Transducers '05 (*311-6 Vol. 1
[21] Happer W, Mathur BS 1967 *Physical Review* **163** 12
[22] Cohen-Tannoudji C, Dupont-Roc J 1972 *Phys Rev A* **5** 968-84
[23] Lee S-K, Romalis MV 2008 *Journal of Applied Physics* **103** 084904
[24] Kornack TW, Smullin SJ, Lee S-K, Romalis MV 2007 *Appl Phys Lett* **90** 223501
[25] Griffith WC, Knappe S, Kitching J 2010 *Optics express* **18** 27167-72
[26] Knappe S, Sander TH, Kosch O, Wiekhorst F, Kitching J, Trahms L 2010 *Appl Phys Lett* **97** 133703
[27] Knappe S, Mhaskar R, Preusser J, Kitching J, Trahms L, Sander T 2012 *5th European Conference of the International Federation for Medical and Biological Engineering (*Springer Berlin Heidelberg) p. 1330-3
[28] Alem O, Sander TH, Mhaskar R, LeBlanc J, Eswaran H, Steinhoff U, et al. 2015 *Phys Med Biol* **60** 4797-811
[29] Sander TH, Preusser J, Mhaskar R, Kitching J, Trahms L, Knappe S 2012 *Biomed Opt Express* **3** 981-90
[30] Ledbetter MP, Savukov IM, Budker D, Shah V, Knappe S, Kitching J, et al. 2008 *Proceedings of the National Academy of Sciences of the USA* **105** 2286-90